TACI-Deficient Macrophages Protect Mice Against Metaflammation and Obesity-Induced Dysregulation of Glucose Homeostasis

Lunhua Liu,[1] Karen Etsuko Inouye,[2] Windy Rose Allman,[1] Adam Steven Coleman,[1] Shafiuddin Siddiqui,[1] Gökhan Siddik Hotamisligil,[2] and Mustafa Akkoyunlu[1]

Transmembrane activator and calcium modulator and cyclophilin ligand interactor (TACI) is a receptor for the TNF superfamily cytokines, B cell–activating factor (BAFF), and A proliferation–inducing ligand (APRIL). Here, we demonstrate that TACI-deficient mice subjected to high-fat diet (HFD) are protected from weight gain and dysregulated glucose homeostasis. Resistance to HFD-induced metabolic changes in TACI-deficient mice does not involve TACI-mediated adipogenesis. Instead, accumulation of M2 macrophages (Mϕs), eosinophils, and type 2 innate lymphoid cells in visceral adipose tissue (VAT) is implicated in the protection from obesity-induced assaults. In support of this hypothesis, adoptively transferred TACI-deficient peritoneal or adipose tissue Mϕs, but not B cells, can improve glucose metabolism in the obese host. Interestingly, the transferred TACI-deficient Mϕs not only home to host VAT but also trigger the accumulation of host M2 Mϕs and eosinophils in VAT. The increase in host M2 Mϕs in VAT is likely a result of eosinophil recruitment in response to eotaxin-2 produced by TACI-deficient Mϕs. Insulin signaling experiments revealed that IL-10 secreted by TACI-deficient Mϕs is responsible for maintaining adipocyte insulin sensitivity. Thus, the adoptive transfer experiments offer a model where TACI-deficient Mϕs accumulate in VAT and protect against metaflammation and obesity-associated dysregulation of glucose metabolism.

The growing epidemic of obesity is increasingly associated with the risk for type 2 diabetes, cardiovascular disease, metabolic syndrome, and cancer (1). In obesity, chronic inflammation within adipose tissue (AT) and other metabolic tissues is a crucial step in the development of insulin resistance and diabetes (2–4). AT inflammation is characterized by abnormal cytokine production and immune cell accumulation, leading to activation of inflammatory signaling pathways. In obese mice, infiltrating T cells and B-2 cells drive the differentiation of AT macrophages (Mϕs) into the insulin resistance–promoting M1 phenotype by secreting interferon-γ and pathogenic IgG, respectively (5,6). Conversely, eosinophils, type 2 innate lymphoid cells (ILC2), regulatory T cells, and Th2 cells in lean mice are involved in the polarization of AT Mϕs toward the anti-inflammatory M2 phenotype by secreting IL-4, IL-13, and IL-10 (5,7). Thus, the shift from M2 to M1 Mϕs within AT during obesity promotes a proinflammatory environment and contributes to the development of systemic insulin resistance (5,8).

Transmembrane activator and calcium modulator and cyclophilin ligand interactor (TACI) is one of the three receptors for the TNF superfamily cytokines, B cell–activating factor (BAFF) and A proliferation–inducing ligand (APRIL) (9). Besides TACI, BAFF and APRIL also share the receptor B-cell maturation antigen, while BAFF receptor belonging to the TNF family engages BAFF. BAFF system molecules play key roles in B- and plasma cell survival, IgG and IgA isotype switch, and antibody production (9,10). Although BAFF and APRIL receptors are primarily expressed in B cells and a subset of T cells, BAFF system molecules are also detected in AT-derived mesenchymal cells, mature adipocytes, and adipose-derived tumors (11). Studies in high-fat diet (HFD)-fed transgenic mice indicated that BAFF knockout (KO) or BAFF receptor–deficient mice manifest

improved glucose tolerance and reduced systemic inflammation compared with wild-type mice (12–14). Paradoxically, despite the improvement in glucose tolerance, weight gain was higher in BAFF KO than wild-type mice after HFD regimen (12). Although BAFF has been shown to adversely affect insulin sensitivity of adipocytes (15), the improvement in glucose tolerance in both these KO mice may also be due to reduced number of mature B cells (9), since B cells fuel inflammation in AT (6). The involvement of TACI in adipogenesis and obesity-induced metabolic changes is not known.

Promotion of HFD-mediated metabolic disease by BAFF system molecules may also involve Mϕs because BAFF and APRIL polarize Mϕs toward the M1 phenotype (16). We recently reported that BAFF and APRIL induce the expression of M1 markers with a concomitant inhibition of M2 markers in Mϕs. Moreover, Mϕs harvested from TACI KO mice manifest the M2 phenotype, and TACI deficiency in Mϕs is responsible for the susceptibility of otherwise resistant C57BL/6 mice to cutaneous *Leishmania* infection (16). Here, we investigated the influence of global TACI deficiency on HFD-associated metabolic changes. We demonstrated that HFD-fed TACI KO mice are mostly protected from weight gain, impaired glucose tolerance, and insulin sensitivity. The M2-skewed phenotype of TACI KO Mϕs is responsible for their resistance to metabolic complications because the transfer of TACI KO Mϕs is sufficient to correct the dysregulated glucose metabolism in obese wild-type mice. These findings highlight the crucial role for TACI-mediated M1 polarization of AT Mϕs and subsequent metaflammation in metabolic complications associated with obesity and present TACI as a novel therapeutic target against obesity-associated diseases such as type 2 diabetes.

RESEARCH DESIGN AND METHODS

Animals and Animal Care
Adult 6- to 8-week-old C57BL/6 and B6.SJL-Ptprca Pepcb/BoyJ mice were purchased from the The Jackson Laboratory (Bar Harbor, ME). TACI KO mice were on C57BL/6 background (10,17). Mice were maintained and bred at the U.S. Food and Drug Administration Animal Research Center following the Animal Research Advisory Committee guidelines. All experiments were performed in female mice, and mouse experiments were approved by the U.S. Food and Drug Administration Institutional Animal Care and Use Committee (protocol 2002-31).

Diet, Body Composition Analysis, and Metabolic Studies
Wild-type and TACI KO female mice were fed either normal chow diet (NCD) (6% fat) or HFD (D12492, 60% kcal fat; Research Diets, New Brunswick, NJ). After 14 weeks, fasting insulin levels were measured with an ultrasensitive mouse insulin kit (Crystal Chem Inc, Downers Grove, IL). For glucose tolerance tests (GTTs), fasted mice were i.p. injected with 1.5 g/kg glucose. For insulin tolerance test (ITTs), mice received 0.5 units/kg human insulin (Sigma-Aldrich, St. Louis, MO), after which blood glucose was measured using the OneTouch Ultra 2 glucose monitoring system (LifeScan, Milpitas, CA). Lean and fat mass compositions were determined by DEXA using a GE Lunar PIXImus densitometer (GE Lunar Corp.). For measurement of VO_2, food intake, and locomotor activity, mice were analyzed using Comprehensive Lab Animal Monitoring System (CLAMS) (Columbus Instruments, Columbus, OH). Mice were allowed to acclimatize for 12 h before measurements were taken. VO_2, VCO_2, and heat measurements were normalized to lean mass or lean and fat mass combined as determined by DEXA analysis at the end of the CLAMS experiment. Subcutaneous AT (SAT) of inguinal fat pad and visceral AT (VAT) of perigonadal fat pad, brown fat pad, and liver of mice were dissected and weighed after euthanasia.

Stromal Vascular Fraction Isolation and Immune Cell Characterization
Perigonadal VATs were minced and digested with type II collagenase (Sigma). Stromal vascular fraction (SVF) cells were obtained as described by Anderson et al. (18). After blocking with anti-CD16/32 antibodies (BD Biosciences, San Jose, CA), cells were stained with fluorophore-conjugated antibodies. Allophycocyanin (APC)-Cy7-B220, APC-TCRβ, phycoerythrin (PE)-Cy7-CD8, PerCP-Cy5.5-CD44, Alexa Fluor 488–CD62L, PE-Cy7-CD45.2, BV421-F4/80, APC-Cy7-CD11c, fluorescein isothiocyanate (FITC)-CD11b, PE–Siglec F, APC-CD11c, Pacific Blue–CD3, Pacific Blue–CD8α, Pacific Blue–CD19, FITC-FCεIα, FITC–Pan NK, APC-Cy7-CD25, PerCP-Cy5-CD127, PE-IL33R, APC-CD11b, Alexa Fluor 488–CD45.1, and PerCP-Cy5.5-CD86 antibodies were from BioLegend (San Diego, CA). FITC-CD4 and eFluor 605-CD4 antibodies were from BD Biosciences and eBioscience (San Diego, CA), respectively. DAPI (Invitrogen, Carlsbad, CA) or 7-aminoactinomycin D (BioLegend) was added as viability dye. Flow cytometry experiments were performed on the BD LSR II and analyzed using FlowJo software (Tree Star, Ashland, OR).

Cell Culture and Preadipocyte Differentiation
For isolation of peritoneal Mϕs, peritoneal exudate cells were harvested and F4/80⁺ cells were purified using the MagniSort Mouse F4/80 Positive Selection Kit (eBioscience). For VAT Mϕ isolation, SVCs were firstly separated with 30 and 70% Percoll gradient and VAT Mϕs were isolated using the F4/80 positive selection kit. Conditioned media (CM) were collected from Mϕs cultured in DMEM/F12 medium for 2 days. 3T3-L1 preadipocytes (American Type Culture Collection, Manassas, VA) and freshly isolated SAT mesenchymal cells were cultured in DMEM. The differentiation and staining of adipocytes were performed as described by Alexaki et al. (11). For BAFF and APRIL stimulation, 100 ng/mL recombinant mouse BAFF (R&D Systems, Minneapolis, MN) or APRIL (Peprotech, Rocky Hill, NJ) was added into differentiation and maintenance medium.

Measurement of Cytokine and Triglyceride Levels

Serum and culture supernatant TNF-α, IL-6, IL-10, and triglyceride levels were quantified by ELISA kits according to the manufacturers' instructions (for TNF-α and IL-6, BD Biosciences; IL-10, R&D Systems; and triglyceride, BioVision, Milpitas, CA).

In Vitro and In Vivo Insulin Sensitization and Immunoblot

SATs from HFD-fed wild-type mice were cut into 1- to 2-mm fractions and cultured for 3 days in VAT Mϕ-CM plus IgG1 or α-IL-10 antibodies (BD Biosciences). Subsequently, the fractions were starved in 0.1% FBS DMEM for 24 h and stimulated with 10 ng/mL insulin for 10 min. Next, proteins were extracted, precipitated, and quantified (19). Anti–phosphorylated (P)-IRS-1 (S1101), IRS-1, P-Akt (S473), Akt, P–extracellular signal–regulated kinase (ERK)1/2 (T202/Y204), total ERK, and goat anti-rabbit IgG antibodies (all from Cell Signaling Technology, Danvers, MA) were used in Western blot analysis.

The effect of Mϕ CM on the sensitivity of SAT to insulin was also analyzed by measuring the insulin receptor (IR) tyrosine kinase activity (20). Briefly, IRs were pulled down from tissue lysates with an anti-IR antibody (0.5 μg/well)–coated plate. The kinase reaction was performed in 100 μL tyrosine kinase assay solution containing peptide substrate IRS-1 (Tyr608) (Enzo Life Sciences, Farmingdale, NY), which was prebiotinylated with EZ-Link NHS-Biotin reagent (Thermo Fisher Scientific, Waltham, MA). The kinase activity was detected with an AlphaScreen P-Tyr-100 Assay kit (PerkinElmer, Waltham, MA) according to the manufacturer's instructions.

For examination of in vivo insulin sensitivity, fasting mice were injected with insulin (10 units/kg body wt) or PBS. Five minutes later, mice were euthanized and skeletal muscle (gastrocnemius), liver, and perigonadal VAT tissues were removed and frozen on dry ice. The frozen tissues were homogenized and solubilized proteins were subjected to Western blot analysis.

For examination of signal transduction in Mϕs, AT Mϕs and peritoneal Mϕs were rested overnight prior to stimulation with APRIL (250 ng/mL) or BAFF (250 ng/mL). In some experiments, 20 nmol/L of the inhibitor, U0126 (InvivoGen), was added 15 min prior to stimulation. At the indicated time points, cells were lysed and subjected to Western blot analysis. Anti–ERK1/2-HRP, anti-P-JAK1 (Y1022/1023), anti-JAK1, anti-JAK2, anti-P-JAK2 (Y1007), anti–STAT1, anti–P-STAT1 (S727), anti-STAT6, anti–β actin-HRP (all from Cell Signaling Technology), and anti–P-STAT6 (Y641) (Abcam, Cambridge, MA) antibodies were used.

Real-time PCR

Total RNA was extracted from sorted VAT Mϕs or 3T3-L1 preadipocytes using the RNeasy Mini Kit (Qiagen, Valencia, CA) or from AT with QIAzol Lysis Reagent (Qiagen). cDNA synthesis and TaqMan gene expression assays were performed as previously described (16).

Immunofluorescence Confocal Microscopy

TACI gene–silenced 3T3-L1 fibroblasts or purified VAT Mϕs were cultured on BD BioCoat Poly-D-lysine/laminin glass coverslips at 10^5 cells/0.5 mL in 24-well plates. Immunofluorescence staining and imaging were performed as previously described (16).

Adoptive Transfer of B Cells and Mϕs

Sorted F4/80$^+$ peritoneal or AT Mϕs were cultured (10^6/mL) for 48 h, after which Mϕs were collected using TrypLE Express Enzyme buffer (Invitrogen). Purity was >95% Mϕs (F4/80$^+$MHCII$^+$Ly6G$^-$) as confirmed by flow cytometry. For B-cell isolation, splenic B cells were purified using the mouse B cell Isolation Kit (Miltenyi Biotec, San Diego, CA). Purified Mϕs and B cells were suspended in PBS, and 5×10^6 cells in 50 μL were injected i.p. into mice.

Eosinophils Chemotaxis Assay

For purification of eosinophils, T and B cells were sequentially depleted from splenocytes using anti-CD90.2 Dynabeads (Thermo Fisher Scientific) and anti-CD19 microbeads (Miltenyi Biotec). Eosinophils stained with Siglec F-PE+ (BD Biosciences) were then enriched with anti-PE microbeads (Miltenyi Biotec). Eosinophil chemotaxis assays were performed as previously described (21).

Statistics

Differences between groups were compared using the Student t test (paired, when applicable) in experiments with $\geq$10 data points and Mann-Whitney U test in experiments with <10 data points. For multiple independent group comparison, two-way ANOVA followed by Bonferroni posttest was performed. GraphPad Prism (La Jolla, CA) software was used for statistical analysis.

RESULTS

TACI Deficiency Protects Mice Against Obesity-Associated Metabolic Changes

To explore the role of TACI in obesity-induced metabolic disease, we first assessed the weight gain in wild-type and TACI KO mice fed the NCD and HFD. Over the course of 14 weeks, HFD-fed TACI KO mice gained significantly less weight than the wild-type mice (Fig. 1A). We next assessed metabolic parameters to gain insight into the difference in weight gain between the mouse strains. When oxygen consumption was normalized to whole body weight, TACI KO mice showed increased energy expenditure compared with wild-type mice. However, this difference was not apparent when the data were normalized to lean body mass, raising the possibility that altered energy expenditure may contribute but may not be the only factor contributing to the decreased weight gain in TACI KO mice (Supplementary Fig. 1A–C). Interestingly, TACI KO mice also manifested significantly more physical activity compared with wild-type mice regardless of the diet (Supplementary Fig. 1D). Food consumption was not a factor in weight gain difference (Supplementary Fig. 1E). Next, we measured parameters associated with glucose homeostasis.
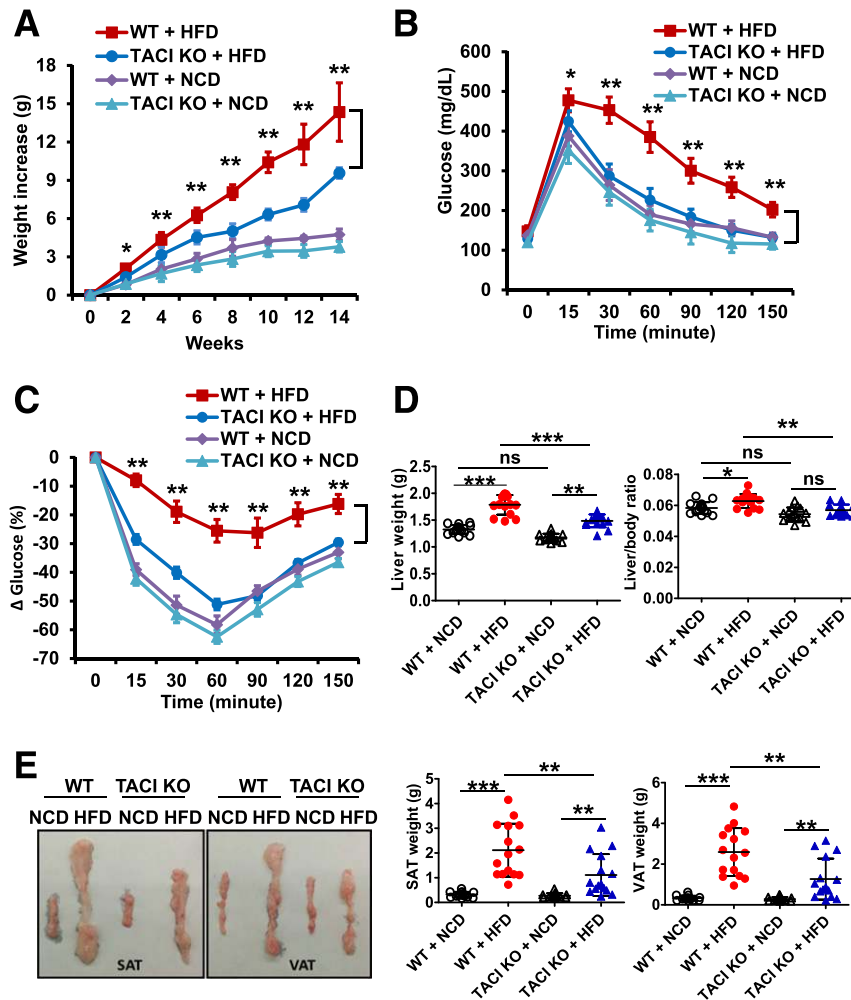
Figure 1—TACI KO mice manifest limited dysregulation in metabolic parameters after HFD feeding. Wild-type (WT) and TACI KO mice were fed with either NCD or HFD (60% kcal fat) for 14 weeks. A: Body weight was measured biweekly to assess weight gain. Intraperitoneal GTT (B) and ITT (C) were performed at 14-week time point. D: Liver, SAT, and VAT of mice were isolated at the end of experiment. E: Liver weight and the ratio of liver to body weight are plotted. A representative image and weights of SAT and VAT from both strains are shown. Data presented as mean ± SD of 15 mice in each group. ns, not significant. *$P < 0.05$; **$P < 0.01$; ***$P < 0.001$.

Although fasting glucose levels were comparable between the two strains, serum insulin levels were significantly lower in HFD-fed TACI KO mice (Supplementary Fig. 2A and B). Importantly, TACI KO mice responded significantly better to glucose challenge in GTT (Fig. 1B) and exhibited improved insulin sensitivity in ITT (Fig. 1C). Moreover, HFD-fed TACI KO mice had lower concentrations of serum IL-6 and TNF-α, two critical inflammatory cytokines associated with type 2 diabetes (2) (Supplementary Fig. 2C and D).

The impairment of insulin sensitivity in obesity is typically accompanied by pathological changes in multiple organs such as liver and AT (22). As expected, HFD-fed wild-type mice had significantly enlarged SAT, VAT (Fig. 1E), and liver (Fig. 1D) compared with TACI KO mice. Elevation in serum lipid levels and fat accumulation in nonadipose tissues is a physiological consequence of high calorie intake (23). We measured significantly reduced accumulation of triglycerides in TACI KO mice liver and

muscle and lower serum levels compared with those of wild-type mice (Supplementary Fig. 2E). Thus, HFD challenge experiments revealed that TACI KO mice resist weight gain and lipid accumulation and are protected against metaflammation, insulin resistance, and glucose intolerance.

TACI KO mice performed better than the wild-type mice in GTT and ITT 14 weeks after the HFD regimen, at which time point there was a significant difference in the body weight between the two strains. For testing of whether the difference in body weight gain contributes to improved metabolic phenotype in TACI KO mice, GTT and ITT were repeated in weight-matched HFD-fed wild-type and TACI KO mice (Supplementary Fig. 3A). Again, TACI KO mice exhibited significantly better glucose tolerance and insulin sensitivity (Supplementary Fig. 3B).

TACI Is Not Involved in Adipogenesis
Next, we analyzed the adipogenic capacity of TACI gene–silenced 3T3-L1 cells because possible involvement of TACI

in BAFF-induced adipogenesis has been proposed (11,24). Immunofluorescence microscopy and real-time PCR analysis indicated that the suppression of TACI protein and mRNA exceeded 50% percent in small interfering RNA (siRNA)-transfected cells (Fig. 2A). We found that neither the proliferation nor the adipogenic capacity of cells was abrogated by the reduction of TACI expression (Fig. 2B and C).

Given that HFD is reported to increase serum and AT BAFF concentrations and BAFF enhances the differentiation of AT-derived mesenchymal cells toward adipocytes (11,24), we assessed BAFF- or APRIL-induced and TACI-mediated adipogenesis in wild-type and TACI KO mouse AT-derived mesenchymal cells. BAFF significantly increased the differentiation of wild-type and TACI-deficient AT-derived mesenchymal cells at the same level (Fig. 2D), while APRIL had no effect on the adipogenesis of these cells. Taken together, these data negate the involvement of TACI in BAFF-dependent or -independent adipocyte differentiation.

TACI KO Mouse AT Cellularity Preserves Type 2 Immunity After HFD Feeding

Upon excess nutrient intake, AT is typically populated with inflammation-promoting immune cells (3,25). Analysis of TCRβ$^+$ cells in the SVF of perigonadal VAT confirmed the accumulation of insulin resistance–promoting CD62L$^-$CD44$^+$ effector memory CD8$^+$ T cells in HFD-fed wild-type mice (Supplementary Fig. 4A). In contrast, the increase in TCRβ$^+$, TCRβ$^+$CD8$^+$, and TCRβ$^+$CD4$^+$ cell numbers remained limited in the VAT of HFD-fed TACI-deficient mice. The population of HFD-fed wild-type mice VAT with B cells was also typical of obese mice (6), and a comparable increase was detected in HFD-fed TACI KO mouse VAT (Supplementary Fig. 4A).

Accumulation of Mϕs and the shift in AT M1/M2 Mϕ balance in favor of M1 phenotype are hallmarks of obesity-induced proinflammatory response (5,26). We confirmed the accumulation of F4/80$^+$ Mϕs, as well as the change in Mϕ composition in favor of F4/80$^+$CD11c$^+$ M1-like Mϕs as compared to F4/80$^+$CD11b$^+$CD11c$^-$ M2-like Mϕs in the AT of HFD-fed wild-type mice (Fig. 3A and Supplementary Fig. 4B). In HFD-fed TACI KO mice, in addition to the limited Mϕ accumulation in VAT, the decrease in M2-like Mϕs was markedly less than in wild-type mice (Fig. 3A and B). Consistent with flow cytometry data, the expression of M1-associated genes (TNFα, NOS, IL6, and MMP9) was higher in sorted wild-type VAT Mϕs than in TACI-deficient Mϕs after HFD feeding (Fig. 3C). In sharp contrast, the expression levels of M2-associated genes (IL10, Arg1, CCL22, IL1RN, YM1, and FIZZ1) were significantly higher in TACI-deficient Mϕs (Fig. 3C). We also measured increased BAFF expression in total VAT of HFD-fed mice, but the increase in wild-type mice was significantly higher than in TACI KO mice (Supplementary Fig. 5A). APRIL expression was only increased in HFD-fed wild-type mice. The level of TACI expression in wild-type AT Mϕs did not change significantly after HFD feeding (Supplementary Fig. 5B and C). The increase in AT BAFF and APRIL expression suggests that these TACI ligands may be contributing to the inflamed milieu through TACI expressed on AT Mϕs in wild-type mice (Supplementary Fig. 5B). Consequently, in the absence of TACI, AT Mϕs likely confer resistance to the HFD-induced metabolic changes by maintaining their M2 phenotype.

Next, we focused on the accumulation of ILC2 and eosinophils in VAT because these cells help sustain M2 Mϕs in VAT (7,27). Although wild-type and TACI KO mice contained similar number of eosinophils in spleen, lung, and peritoneal cavity (Supplementary Fig. 6A), under the NCD regimen TACI KO mouse VAT contained significantly more CD11b$^+$Siglec F$^+$ eosinophils and CD127$^+$CD25$^+$IL33R$^+$ ILC2 cells than wild-type mice (Fig. 3D and E and Supplementary Fig. 6B and C). HFD feeding led to a reduction in eosinophil and ILC2 frequency in both mouse groups, but the numbers in TACI KO mice were significantly higher than those of wild-type mice (Fig. 3D and E). Thus, the association among ILC2, eosinophils, and M2 Mϕs in lean AT (7,27) was also observed in the VAT of HFD-fed TACI KO mice.

ERK and STAT1 Signal Pathways Are Involved in BAFF- and APRIL-Induced Polarization of Mϕs

Characterization of AT Mϕs in HFD-fed mice suggested a resistance to the switch to the inflammatory M1 phenotype when TACI is absent. Using peritoneal Mϕs, we previously showed that BAFF and APRIL can drive the inflammatory Mϕ phenotype through ERK1/2 (16). Other molecules involved in M1 polarization of Mϕs include STAT1, JAK1, JAK2, and STAT6 (28,29). For assessment of whether BAFF and APRIL activate these molecules in peritoneal Mϕs, we measured the phosphorylation of STAT1, JAK1, JAK2, and STAT6 in Western blot analysis. In addition to ERK1/2, STAT1 phosphorylation was enhanced in wild-type Mϕs with BAFF and APRIL stimulation, while others were not (Supplementary Fig. 7A). Implicating a role for TACI, both ERK1/2 and STAT1 phosphorylations were severely attenuated in stimulated TACI-deficient Mϕs. The activation of ERK1/2 and STAT1 by TACI ligands was not restricted to peritoneal Mϕs; BAFF and APRIL treatment also induced the phosphorylation of ERK1/2 and STAT1 in AT Mϕs of NCD- and HFD-fed wild-type mice (Fig. 4A). As expected, ERK1/2 and STAT1 phosphorylations were ablated in BAFF- or APRIL-treated AT Mϕs of TACI KO mice regardless of their diet.

Using peritoneal Mϕs, we previously showed that TACI-mediated ERK1/2 activation governs the M1 polarization of Mϕs because APRIL-induced IL-6, MMP-9, and CD80 upregulation could be ablated by U0126, a small-molecule inhibitor specific for ERK1/2 (16). To test whether STAT1 is involved in BAFF- and APRIL-induced M1 polarization, we silenced the STAT1 gene in wild-type peritoneal Mϕs with siRNA targeting STAT1 (Fig. 4B). Reduction in STAT1 significantly ablated the BAFF- and APRIL-induced
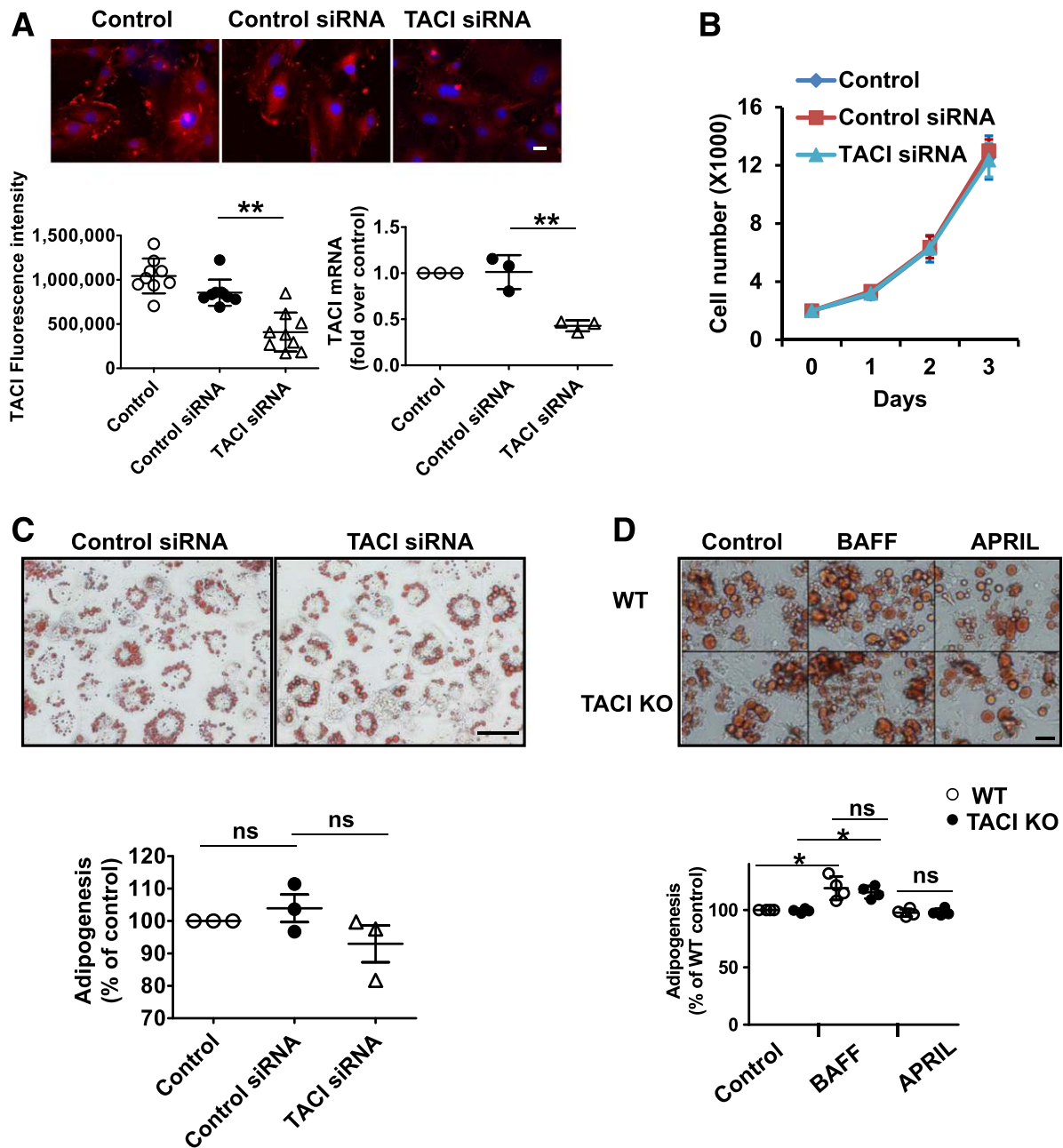
Figure 2—TACI is not required for adipogenesis. *A*: TACI expression in 3T3-L1 fibroblasts was determined by confocal microscope (scale bar = 20 μm) or real-time PCR 48 h after transfection of cells with control or TACI-specific siRNA. The samples were run in duplicates, and each experiment was repeated three times. Quantification of TACI (red) fluorescence intensity and mRNA levels were plotted. **$P < 0.01$. *B*: The proliferation of control or TACI-specific siRNA–transfected 3T3-L1 fibroblasts was quantified by counting the live cells after exclusion of the trypan blue–stained dead cells. The samples were run in triplicates, and each experiment was repeated three times. *C*: Control or TACI-specific siRNA–transfected 3T3-L1 cells were incubated with differentiation medium for 3 days and maintenance medium for another 3 days. Cells were fixed and lipid accumulation was monitored by Oil Red O staining. Images are presented at original magnification ×200 (scale bar = 100 μm). Lipid stains were extracted with isopropyl alcohol and quantified with spectrophotometry. Data were normalized to the mock control, and means ± SD of three experiments were plotted. *D*: Wild-type (WT) and TACI KO primary SAT-derived mesenchymal cells, isolated from groups of three mice, were incubated with differentiation medium for 3 days and maintenance medium for 3 more days with or without 100 ng/mL BAFF or APRIL. Cells were fixed and lipid accumulation was monitored by Oil Red O staining. Images are presented at original magnification ×200 (scale bar = 50 μm). Lipid stains were extracted with isopropyl alcohol and quantified with spectrophotometry. Data were normalized to the wild-type control, and the means ± SD of four experiments were plotted. ns, not significant. *$P < 0.05$.

expression of genes for IL-6, MMP-9, NOS2, and TNF-α (Fig. 4*C*), as well as the proteins for CD80 and CD86 (Supplementary Fig. 7*B*). As show in Fig. 4*B*, silencing of

the STAT1 gene efficiently ablated STAT1 and P-STAT1 but did not change the phosphorylation of ERK1/2, while inhibition of ERK1/2 with U0126 resulted in the attenuation
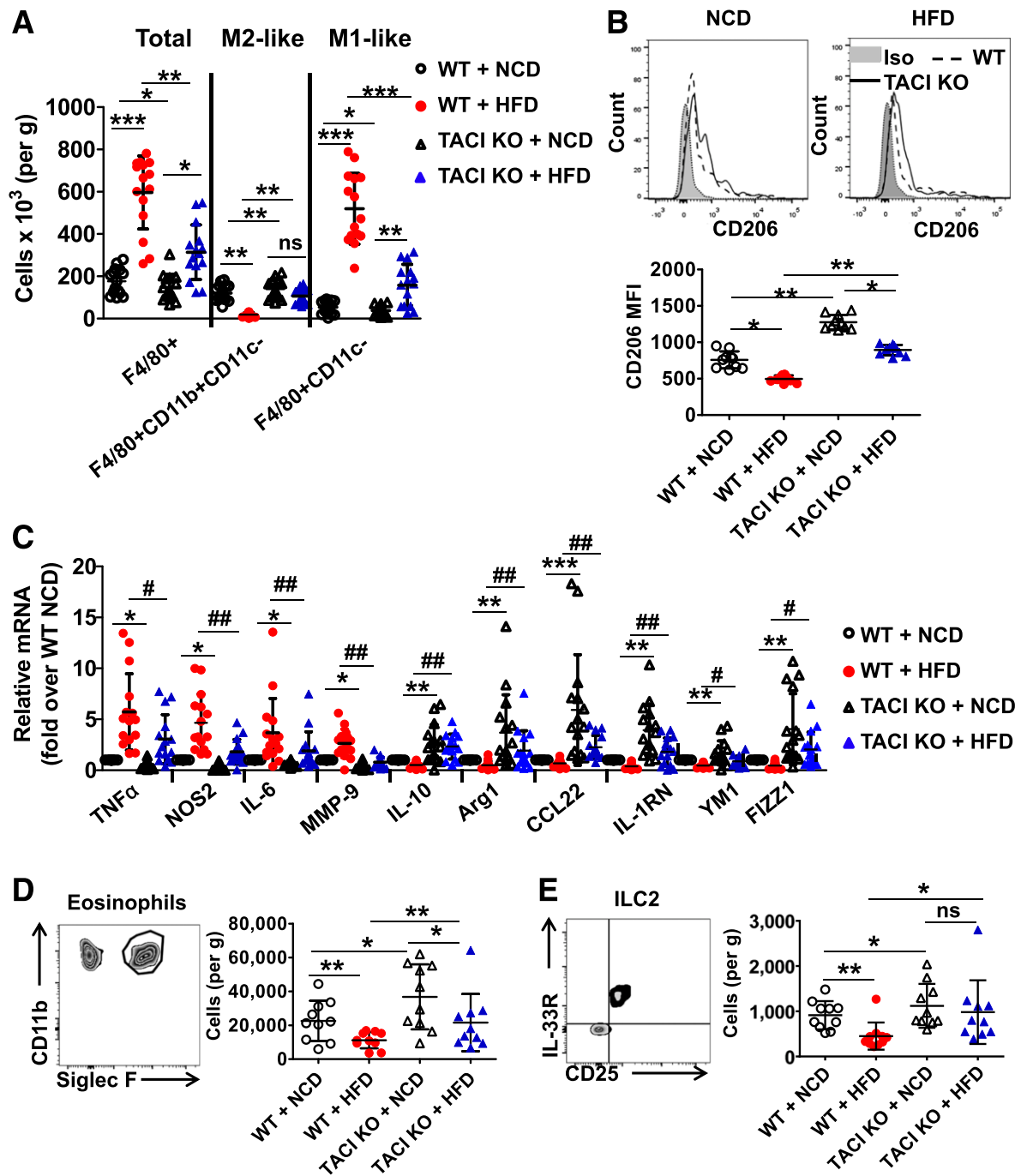
Figure 3—Changes in TACI KO mouse AT cellular composition after HFD challenge reflect type 2 immune response. A: TACI KO and wild-type (WT) mouse SVF cells were isolated from perigonadal fat pad and analyzed by flow cytometry. Isolated cells were stained with F4/80, CD11b, and CD11c antibodies to enumerate M1-like and M2-like Mϕs. (See Supplementary Fig. 3B for gating strategy.) Data presented as mean ± SD of 15 mice. B: SVF cells were further purified by density centrifugation with 30 and 70% Percoll gradient, and Mϕs were positively collected using F4/80 antibodies and magnetic-activated cell sorting technology. CD206 expression on isolated Mϕs was measured by flow cytometry. Data presented as mean ± SD of 10 mice. C: Isolated Mϕs were also used to quantify the expression levels of M1- and M2-associated genes in real-time PCR. Data presented as mean ± SD of 15 mice per group. D: Perigonadal fat pad SVF cells were gated with CD11b and Siglec F antibodies to quantify eosinophil numbers. (See Supplementary Fig. 5B for gating strategy.) Data presented as mean ± SD of 10 mice. E: Antibodies against CD25, CD127, and IL-33R molecules were used to quantify ILC2 cells. (See Supplementary Fig. 5C for detailed gating strategy.) Data presented as mean ± SD of 10 mice. Quantification of Mϕs, eosinophils, and ILC2 was shown as cell numbers of fluorophore-positive cells in 1 g of VAT tissue. Iso, isotype; MFI, mean fluorescence intensity; ns, not significant. *$P < 0.05$, **$P < 0.01$, and ***$P < 0.001$. #$P < 0.05$ and ##$P < 0.01$.

of both ERK1/2 and STAT1 phosphorylation induced by BAFF and APRIL (Supplementary Fig. 7C). These observations suggested that ERK1/2 functions upstream of STAT1. Thus, in HFD-fed TACI KO mice, the ablation of BAFF- and APRIL-induced phosphorylation of ERK1/2 and STAT1 likely prevents the M1 polarization of AT Mϕs.
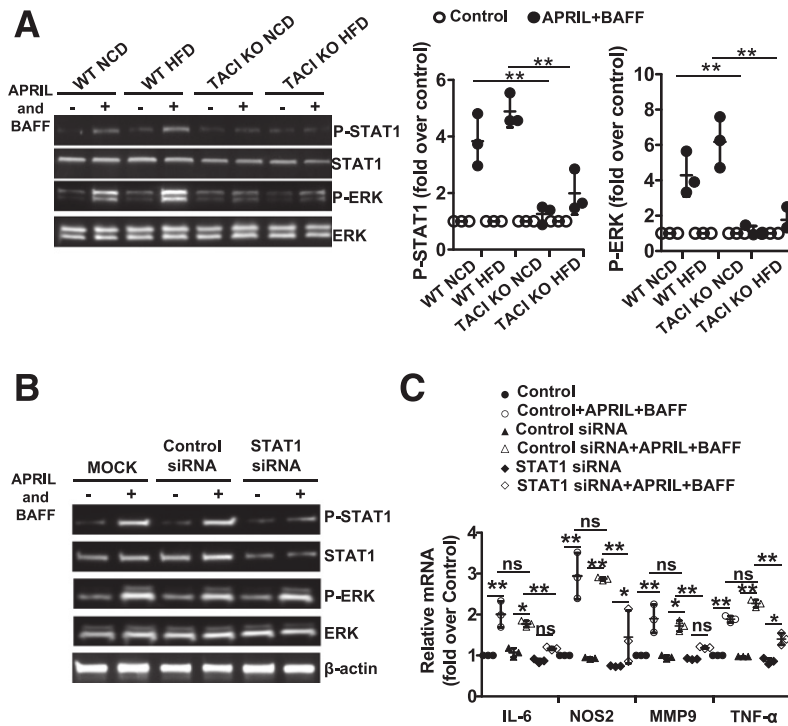
Figure 4—Impaired BAFF- and APRIL-induced ERK/STAT1 signaling is responsible for the M2 polarization of TACI-deficient Mφs. A: AT Mφs from TACI KO or WT HFD mice were stimulated with APRIL plus BAFF for 24 h. Total and phosphorylated ERK1/2 and STAT1 were detected by Western blot analysis. One out of three experiments with similar results is shown. B: Peritoneal Mφs from wild-type (WT) mice were stimulated with APRIL plus BAFF for 24 h after transfection with control or STAT1 siRNA. Total and phosphorylated forms of STAT1 and ERK1/2 were detected by Western blot analysis. One out of three experiments with similar results is shown. C: The expression of M1-associated genes in these cells was analyzed by real-time PCR. Data presented are the mean ± SD of three experiments. ns, not significant. *$P < 0.05$, **$P < 0.01$.

Transfer of TACI KO Mφs Is Sufficient to Improve Glucose Homeostasis in Obese Recipient Wild-Type Mice

Since Mφs are important contributors to the protection afforded by type 2 immune response in AT (30), and TACI influences the Mφ phenotype, AT cellular composition analysis experiments suggested a role for M2-skewed Mφs in the protection of TACI KO mice from HFD-induced metabolic disease. However, the global KO mouse used in our experiments prevents us from excluding the participation of other cell types in the resistance of the TACI KO mouse to HFD-induced metabolic disease. To exclude the contribution of host genetic factors, and to definitively examine the role of TACI-deficient Mφs, we performed adoptive transfer experiments. We preferred adoptive transfer experiments to bone marrow chimera experiments because a recent study reported that circulating monocytes and tissue Mφs exhibit M2-skewed phenotype after bone marrow transplantation (31). The increase in the inflammatory Mφ population in AT is primarily attributed to the chemokine-induced accumulation of monocytes from the periphery, although more recent reports suggest the contribution by the proliferation of local tissue resident Mφs also (32,33). We used peritoneal Mφs from HFD-fed mice to understand the impact of peripheral Mφs

on established metabolic changes in obese wild-type mice. We began by assessing the glucose metabolism in obese wild-type mice after the transfer of Mφs from HFD-fed TACI KO or wild-type mice. TACI KO mice that received Mφs from HFD-fed wild-type or TACI KO mice served as control. Two weeks after the transfer of TACI-deficient Mφs, HFD-fed wild-type mice exhibited lower blood insulin, IL-6, and TNF-α levels than the PBS-injected group (Fig. 5A–C). In sharp contrast, mice that received wild-type Mφs had increased serum insulin, IL-6, and TNF-α compared with PBS-injected mice. No remarkable change in brown fat, liver, SAT, or VAT weights or in basal blood glucose level was detected in these mice (Supplementary Fig. 8A and B). Recipients of TACI-deficient Mφs gained significantly less weight than those that received PBS at 2 and 4 weeks after Mφ transfer (Fig. 5D). Wild-type Mφs transferred into HFD-fed wild-type mice aggravated insulin resistance in the recipient mice, though without a substantial impact on glucose tolerance (Fig. 5E). By contrast, recipients of TACI-deficient Mφs manifested significantly improved glucose tolerance and insulin resistance compared with PBS-injected mice (Fig. 5E). Similar effects of donor Mφs were observed in TACI KO recipient mice, albeit with greater influence of wild-type Mφs in worsening glucose tolerance and insulin sensitivity
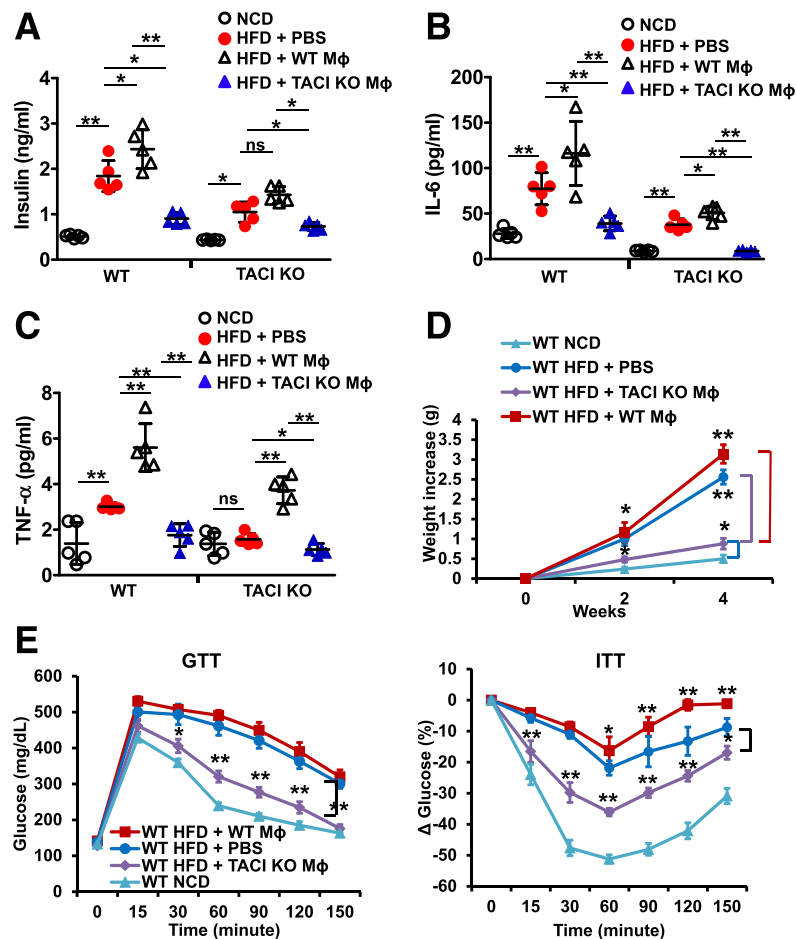
Figure 5—Transfer of TACI-deficient Mφs improves glucose homeostasis in obese wild-type (WT) mice. Peritoneal Mφs were isolated from HFD-fed WT or TACI KO mice and transferred into either HFD-fed WT or TACI KO recipient mice. NCD-fed mice and PBS-injected mice served as controls. After 14 days, basal serum insulin (A), IL-6 (B), and TNF-α (C) levels were assessed. *D*: The increase in body weight 2 and 4 weeks after the transfer of peritoneal Mφs or PBS was determined. NCD-fed WT mice served as control. *E*: Intraperitoneal GTT and ITT were also performed 14 days after Mφ transfer. Data presented as mean ± SD of five mice per group. In GTT and ITT groups, statistical comparisons were made with PBS-injected HFD-fed WT mice. ns, not significant. *$P < 0.05$; **$P < 0.01$.

than the beneficial effect of TACI-deficient Mφs on these parameters (Supplementary Fig. 8*C*).

Given the significance of TACI in B-cell hemostasis and the role of B cells in regulating insulin sensitivity in VAT (6,9), we also examined the influence of TACI-deficient B cells in the resistance of TACI KO mice to obesity-induced dysregulation of glucose homeostasis. B-cell adoptive transfer experiments revealed that B cells from HFD-fed TACI KO or wild-type mice did not alter the metabolic disease parameters in obese wild-type mice (Supplementary Fig. 9).

Next, we sought to determine whether Mφs isolated from the AT of mice exposed to high calorie intake would also alleviate the metabolic dysfunction in obese wild-type mice. As in peritoneal Mφ-transfer experiments, transfer of Mφs isolated from the AT of HFD-fed TACI KO mice improved the glucose and insulin tolerance of obese wild-type mice 2 weeks after the transfer (Supplementary Fig. 10*A*). Also resembling the results of peritoneal Mφ-transfer

experiments, adoptively transferring TACI-deficient AT Mφs decreased the serum insulin concentrations (Supplementary Fig. 10*B*). Mφs isolated from the wild-type AT, on the other hand, did not impact the metabolic parameters in the recipient mice (Supplementary Fig. 10*A*). Taken together, the adoptive transfer experiments indicated that TACI-deficient Mφs are responsible for the resistance of TACI KO mice to the development of metabolic disease in response to high calorie intake.

Anti-inflammatory Cells Populate the Obese Mouse VAT After TACI KO Mφ Transfer

Next, we explored whether adoptively transferred Mφs modify recipient mouse VAT cellular composition. First, we determined that CD45.1[+] donor Mφs could populate the VAT of CD45.2[+] recipient mice (Supplementary Fig. 11*A*). Assessments made 14 days after the transfer indicated that injection of Mφs from HFD-fed wild-type mice
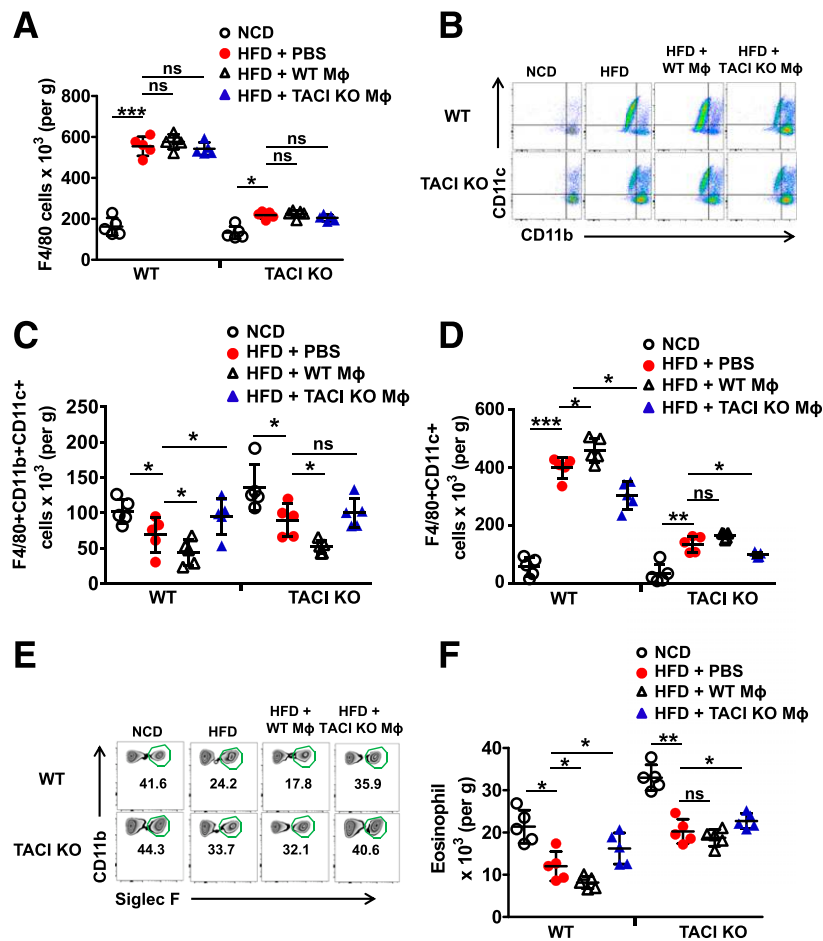
Figure 6—Populations of M2-like Mφs and eosinophils increase in obese wild-type (WT) mouse VAT after the adoptive transfer of TACI-deficient Mφs. Peritoneal Mφs were isolated from HFD-fed WT or TACI KO mice and transferred into either HFD-fed WT or TACI KO recipient mice. NCD-fed mice and PBS-injected mice served as controls. After 14 days, SVF cells were isolated from VAT of WT and TACI KO recipient mice and analyzed by flow cytometry. F4/80$^+$ Mφs (A) were gated, and CD11b$^+$CD11c$^-$ or CD11c$^+$ subpopulations (B) were quantified (C and D). Eosinophils of VAT were also analyzed and quantified based on Siglec F and CD11b staining (E and F). Data presented as mean ± SD of five mice per group. ns, not significant. *P < 0.05, **P < 0.01, and ***P < 0.001.

resulted in a significant increase in F4/80$^+$CD11c$^+$ Mφs while decreasing the number of F4/80$^+$CD11b$^+$CD11c$^-$ Mφs in either recipient mouse without changing the total number of VAT Mφs (Fig. 6A–D). By contrast, Mφs from HFD-fed TACI KO mice significantly increased the population of F4/80$^+$CD11b$^+$CD11c$^-$ anti-inflammatory Mφs and decreased the F4/80$^+$CD11c$^+$ proinflammatory Mφs in the VAT of either recipient mouse (Fig. 6C and D). To define the source of M2-like Mφs that populate the VAT after TACI-deficient Mφ transfer, we transferred CD45.2$^+$ Mφs from HFD-fed TACI KO mice into CD45.1$^+$ HFD-fed wild-type mice. Two weeks after the transfer, ~18% of the VAT Mφs in the host were CD45.2$^+$ TACI-deficient cells (Supplementary Fig. 11B and C). Moreover, these cells maintained their M2 phenotype in the host VAT, as evidenced by lower expression of CD86 and higher expression of CD206 molecules (Supplementary Fig. 11B and D). Interestingly, compared with PBS-injected mice, CD45.1$^+$ host VAT Mφs also expressed significantly lower levels

of CD86 and higher levels of CD206 after the transfer of TACI KO Mφs, suggesting a switch to M2 phenotype of these Mφs (Supplementary Fig. 11D). Thus, the transferred TACI-deficient Mφs not only preserved their M2 phenotype in the host but were also able to influence the phenotype of host VAT Mφs.

Analysis of other cell types in the recipient mouse VAT indicated that numbers of ILC2, CD4$^+$, and CD8$^+$ T cells as well as their activated subsets remained unchanged after the transfer of Mφs (Supplementary Fig. 12A–C). However, wild-type Mφs decreased and TACI-deficient Mφs increased eosinophil numbers in the recipient mice compared with PBS-injected mice (Fig. 6E and F). TACI-deficient Mφs are likely responsible for the population of host VAT with eosinophils because we measured significantly higher expression of the eosinophil chemotactic factor, eotaxin-2 (34), in VAT-resident TACI-deficient Mφs than wild-type Mφs (Fig. 7A), and CM from TACI-deficient VAT Mφs induced significantly

A

B
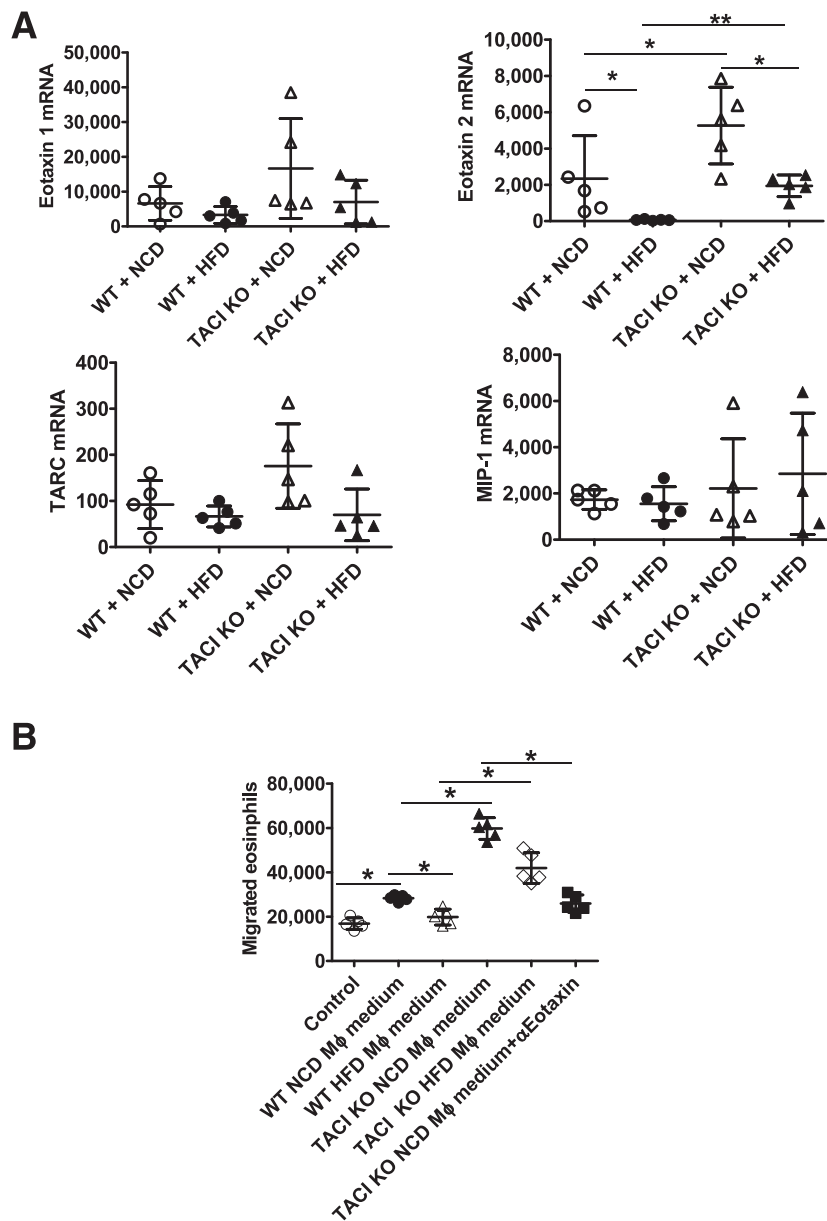
Figure 7—Expression of eosinophil chemotactic factors by VAT and chemotaxis of eosinophils induced by CM from VAT Mφs. *A*: SVF cells of HFD- or NCD-fed wild-type (WT) or TACI KO mice were purified by density centrifugation with 30 and 70% Percoll gradient. Mφs were positively collected using anti-F4/80 antibodies and MACS technology. Eotaxin-1, eotaxin-2, TARC, and MIP-1β mRNA were quantified in real-time PCR. Data presented as mean ± SD of five mice. *B*: Splenic eosinophils (2×10^5 per Transwell insert) were placed into the upper chamber of Transwell plate with DMEM/F12 "control" medium or CM from VAT Mφs in the lower chamber and incubated at 37°C for 2 h. For neutralization of eotaxin-2, CM were incubated at room temperature with 2 μg/mL anti–eotaxin-2 antibody for 30 min. Total numbers of live cells that had migrated into the lower side of insert and the bottom chamber were counted. Data presented as mean ± SD of five mice. *$P <$ 0.05; **$P <$ 0.01.

more eosinophil chemotaxis than CM of wild-type Mφs, which was inhibited by a neutralizing anti–eotaxin-2 antibody (Fig. 7*B*). The other eosinophil-related chemokines eotaxin-1, thymus and activation-induced chemokine (TARC), and Mφ inflammatory protein (MIP)-1β (34) were not likely to be involved in the recruitment of eosinophils because their levels were not elevated in TACI KO Mφs (Fig. 7*A*).

Insulin Sensitivity Is Preserved in HFD-Fed TACI KO Mice, and the VAT Mφs From TACI KO Mice Enhance Insulin Sensitivity of Adipocytes

Increased secretion of TNF-α and IL-6 and reduced release of IL-10 by AT Mφs are detrimental to insulin signaling (2,35). Our adoptive transfer experiments pointed to the M2-skewed TACI-deficient Mφs and the anti-inflammatory cytokines secreted by them as the plausible
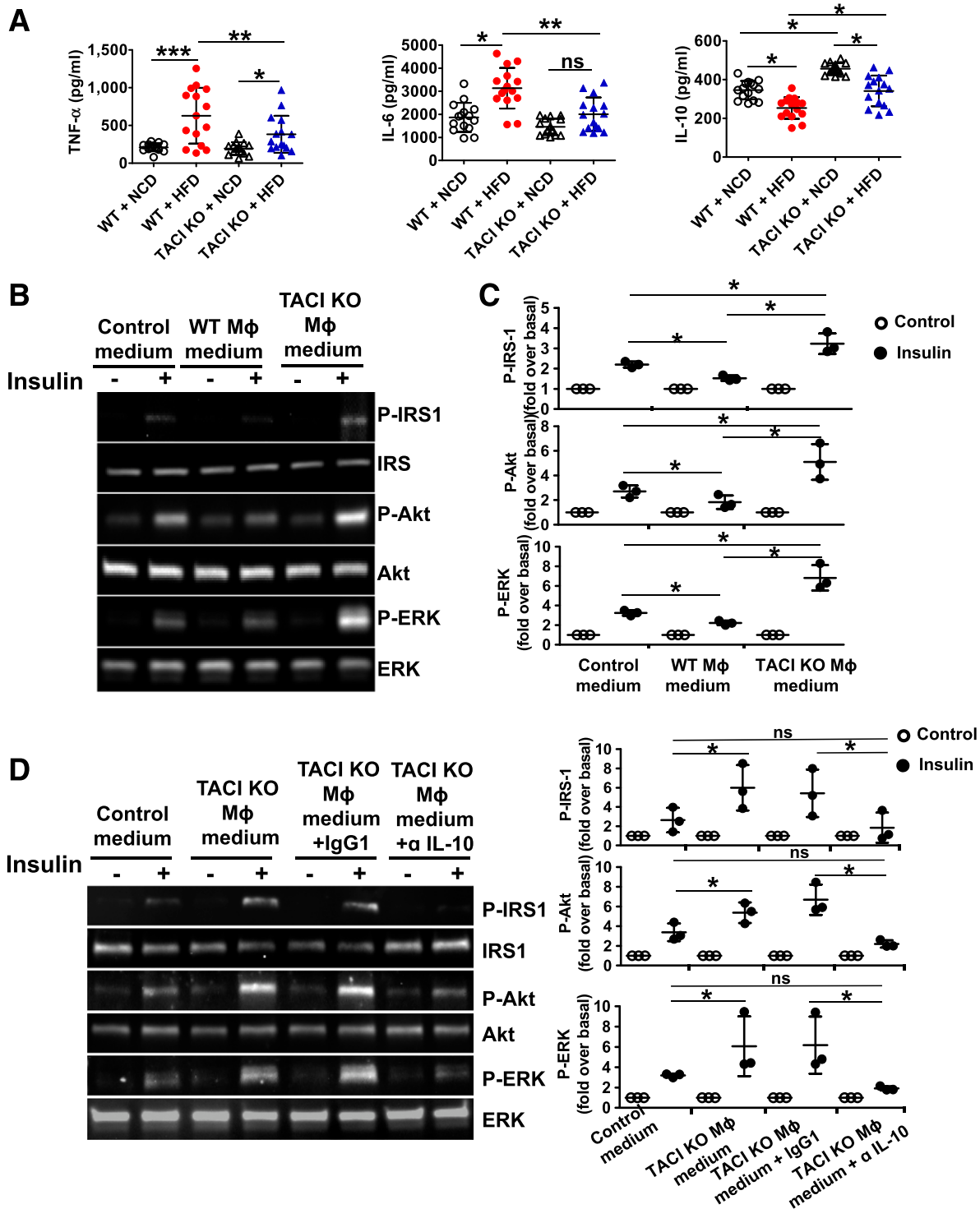
Figure 8—TACI-deficient Mφs sensitize wild-type (WT) adipocytes to insulin stimulation. A: Mean TNF-α, IL-6, and IL-10 levels in culture supernatants of WT and TACI-deficient VAT Mφs are shown (n = 15 for each group). B: HFD-fed WT mouse SAT fractions were cultured in CM collected from VAT Mφs of HFD-fed WT or TACI KO mice for 3 days and then starved for 24 h. After starvation, cells were stimulated with insulin and extracted proteins were subjected to Western blot analysis. One of three experiments with similar results is shown. C: Ratios of P-IRS-1, P-Akt, and P-ERK1/2 band densities in CM-stimulated VAT fractions to their corresponding total proteins were calculated. Mean fold induction relative to basal levels from three experiments is shown. D: WT mouse VAT fractions were cultured for 3 days in CM from HFD-fed TACI-deficient Mφs with IgG1 or α-IL-10 antibodies. After 3 days of starvation and insulin stimulation, proteins were extracted and subjected to Western blot analysis. One of three experiments with similar results is shown. ns, not significant. *P < 0.05; **P < 0.01; ***P < 0.001.

mechanism for the resistance of HFD-fed TACI KO mice to metabolic disease. Supporting this hypothesis, we found elevated levels of TNF-α and IL-6 in the culture supernatants of HFD-fed wild-type mouse Mφs compared with those of TACI KO mice (Fig. 8A). More importantly, both the NCD- and HFD-fed TACI-deficient Mφ CM contained significantly higher levels of IL-10 (Fig. 8A). Since IL-10, TNF-α, and IL-6 directly influence the responses of adipocytes to insulin (2,35), we probed the effects of CM from TACI KO and wild-type mice Mφs on the sensitivity of AT to insulin. As expected (36), CM from wild-type Mφs significantly suppressed insulin-induced phosphorylation of IRS-1, ERK1/2, and Akt compared with cells stimulated with insulin in control media (Fig. 8B and C). By contrast, insulin induced a robust phosphorylation of IRS-1, ERK1/2, and Akt in cells incubated with CM from TACI-deficient Mφs. Moreover, the insulin-sensitizing activity of CM from TACI-deficient Mφs could be abrogated by an IL-10–neutralizing antibody (Fig. 8D). These results were corroborated in IR kinase activity assay, where we measured higher levels of tyrosine kinase activity in lysates of SAT stimulated with TACI-deficient Mφ-CM than those stimulated with CM from wild-type Mφs (Supplementary Fig. 13A). Moreover, the IR kinase activity elicited by CM from TACI-deficient Mφs was significantly inhibited by anti–IL-10 antibodies. Similarly, CM from TACI-deficient Mφs potentiated insulin signaling in 3T3-L1 differentiated adipocytes (Supplementary Fig. 13B and C). Promotion of insulin sensitivity in adipocytes by TACI-deficient Mφs suggested that enhanced insulin sensitivity in metabolically important organs is likely responsible for the improved ITT in HFD-fed TACI KO mice. To test this hypothesis, we measured Akt phosphorylation in liver, muscle, and VAT of HFD-fed mice after insulin injection. As expected (37), all three tissues of HFD-fed wild-type mice demonstrated impaired Akt phosphorylation after insulin injection (Supplementary Fig. 14A and B). In contrast, Akt phosphorylation levels remained high in all three TACI KO mouse tissues after HFD feeding. Thus, preservation of IR-transduced signaling strength by molecules secreted from Mφs (such as IL-10) is responsible for the protection of TACI KO from HFD-induced glucose dysregulation.

DISCUSSION

Using an HFD-induced metabolic disease model, we uncovered a direct role for TACI in the development of obesity-mediated inflammation and dysregulation of glucose metabolism. The TACI KO mice not only were protected against HFD-induced metaflammation, obesity, and insulin resistance but also manifested reduced weight gain. We excluded a BAFF-dependent or -independent role for TACI in the differentiation of precursor cells toward mature adipocytes. Thus, unlike in BAFF- or BAFF receptor–deficient mice (15,24), the resistance of TACI KO mice to metabolic disease is independent of a role for TACI expressed in adipocytes. Instead, the M2 phenotype of TACI-deficient Mφs is likely

to be responsible for maintaining systemic glucose homeostasis by preventing inflammation in AT, which is independent of weight gain as illustrated in weight-matched animals and through adoptive transfer experiments.

In TACI KO mice, higher energy expenditure may be responsible for the limited weight gain after HFD feeding, although we cannot rule out contributions by other factors, since energy expenditure per lean body weight did not differ between wild-type and TACI KO mice. A correlation between reduced energy expenditure and decreased weight gain has been reported for other mouse strains in which M2-polarized Mφs are responsible for improved glucose metabolism (7,38). We also observed increased locomotor activity in TACI KO mice independent of diet. Although the reasons for the heightened physical activity are not known, requiring further investigation, the contribution of activity to higher energy expenditure in TACI KO mice is likely limited because both human and rodent studies have shown that unlike in acute exercise, energy expenditure decreases after longer-term training as a result of compensatory mechanisms such as muscle efficiency (39,40). Supporting this hypothesis, there was no weight difference between NCD-fed TACI KO and wild-type mice despite increased physical activity in TACI KO mice.

The overall cellular composition of HFD-fed TACI KO mouse AT shares similarities with that of lean mice, especially in regard to elevated numbers of M2-skewed Mφs, eosinophils, and ILC2 (5,7,27). Adoptive transfer experiments with peritoneal and AT Mφs solidified the role of TACI-deficient Mφs in alleviating obesity-related dysregulation of glucose tolerance and insulin resistance. Interestingly, cellularity analysis in host AT indicated that the donor TACI-deficient Mφs not only maintained their M2 status in the host AT but also promoted in situ increase of host M2 Mφs (Supplementary Fig. 15). Elevated number of host M2 Mφs in AT is likely a result of the increase in eosinophil population, since eosinophils promote M2 polarization of Mφs by secreting IL-4 (27). Accumulation of eosinophils in AT after the transfer of TACI-deficient Mφs is especially interesting because Wu et al. (27) suggested a hierarchal relationship between eosinophils and Mφs, where the recruitment of eosinophils by ILC2 to the lean AT facilitates the polarization of AT Mφs toward the M2 phenotype through secretion of IL-4 and IL-13 (7). In adoptive transfer experiments, we demonstrated that wild-type mouse AT was populated with eosinophils after the transfer of TACI-deficient Mφs. The fact that anti–eotaxin-2 antibodies could block the chemotaxis of eosinophils induced by TACI-deficient Mφs suggests that M2 Mφs participate in the accumulation of eosinophils in AT (27).

Using peritoneal Mφs, we previously demonstrated that TACI mediates M1-polarizing signals through an ERK1/2 pathway (16). In this study, analysis of signaling in AT Mφs confirmed the role of an ERK1/2 pathway in M1 polarization and identified the involvement of STAT1 downstream of ERK1/2. The phosphorylation of both

these molecules was abrogated in BAFF- and APRIL-stimulated TACI-deficient Mϕs, which maintained their M2 phenotype.

The TACI-deficient strain used in our studies has elevated B-cell numbers compared with wild-type mice (41). However, the potentially harmful consequence of elevated B-cell lymphoproliferation is likely mitigated by a concomitant reduction in immunoglobulin levels associated with the prominent role for TACI in the development of plasma cells (9,10,41). A beneficial effect of B-cell lymphoproliferation due to a proportional increase in the number of protective TGF-β– and IL-10–secreting B cells is also not expected in TACI KO mice because TACI mediates BAFF-induced expansion of IL-10–expressing B cells (42). Adoptive transfer experiments confirmed the absence of a protective role for TACI-deficient B cells in HFD-induced dysregulation of glucose metabolism.

Conditioned media from TACI-deficient Mϕs contained lower levels of TNF-α and IL-6 and a higher level of IL-10 than those of wild-type Mϕs. M2 Mϕs are believed to promote insulin sensitivity by blocking the effects of inflammatory cytokines such as TNF-α through the production of anti-inflammatory cytokines, such as IL-10 (43). Indeed, CM from HFD-fed TACI-deficient Mϕs enhanced insulin-induced IRS, Akt, and ERK1/2 phosphorylation, whereas media from HFD-fed wild-type Mϕs suppressed insulin signaling (Supplementary Fig. 15).

In conclusion, we identified a unique role for TACI in promoting obesity and insulin resistance by mediating signals that support the polarization of AT Mϕs toward the M1 phenotype. Our results are consistent with a spectrum of studies recognizing AT accumulated M1 Mϕs as the main source of proinflammatory cytokines that block insulin signaling and the M2 Mϕs as the source of anti-inflammatory cytokines that promote insulin sensitivity (30,44–49). The therapeutic outcome in obese wild-type mice after TACI-deficient Mϕ transfer provides proof of concept in targeting TACI to improve symptoms associated with metabolic disease. TACI inhibition strategies may rely on neutralizing TACI ligands with the help of soluble TACI-fc molecule, although safety can be a concern with systemic inhibition of TACI ligands (50). The use of inhibitory peptides targeting signaling molecules downstream of TACI can be a safer alternative because selective inhibition of TACI is expected to allow the B cells to receive the crucial survival signals mediated by BAFF–BAFF receptor interaction (9). Finally, Mϕ transfer experiments also suggest that the injection of in vitro M2-polarized monocytes into patients with type 2 diabetes may offer therapeutic benefits.

References

1. O'Neill S, O'Driscoll L. Metabolic syndrome: a closer look at the growing epidemic and its associated pathologies. Obes Rev 2015;16:1–12

2. Hotamisligil GS. Inflammation and metabolic disorders. Nature 2006;444:860–867

3. Mathis D. Immunological goings-on in visceral adipose tissue. Cell Metab 2013;17:851–859

4. Uysal KT, Wiesbrock SM, Marino MW, Hotamisligil GS. Protection from obesity-induced insulin resistance in mice lacking TNF-alpha function. Nature 1997;389:610–614

5. McLaughlin T, Ackerman SE, Shen L, Engleman E. Role of innate and adaptive immunity in obesity-associated metabolic disease. J Clin Invest 2017;127:5–13

6. Winer DA, Winer S, Shen L, et al. B cells promote insulin resistance through modulation of T cells and production of pathogenic IgG antibodies. Nat Med 2011;17:610–617

7. Molofsky AB, Nussbaum JC, Liang HE, et al. Innate lymphoid type 2 cells sustain visceral adipose tissue eosinophils and alternatively activated macrophages. J Exp Med 2013;210:535–549

8. Hotamisligil GS. Inflammation, metaflammation and immunometabolic disorders. Nature 2017;542:177–185

9. Sakai J, Akkoyunlu M. The role of BAFF system molecules in host response to pathogens. Clin Microbiol Rev 2017;30:991–1014

10. Kanswal S, Katsenelson N, Selvapandiyan A, Bram RJ, Akkoyunlu M. Deficient TACI expression on B lymphocytes of newborn mice leads to defective Ig secretion in response to BAFF or APRIL. J Immunol 2008;181:976–990

11. Alexaki VI, Notas G, Pelekanou V, et al. Adipocytes as immune cells: differential expression of TWEAK, BAFF, and APRIL and their receptors (Fn14, BAFF-R, TACI, and BCMA) at different stages of normal and pathological adipose tissue development. J Immunol 2009;183:5948–5956

12. Kim DH, Do MS. BAFF knockout improves systemic inflammation via regulating adipose tissue distribution in high-fat diet-induced obesity. Exp Mol Med 2015;47:e129

13. Kawasaki K, Abe M, Tada F, et al. Blockade of B-cell-activating factor signaling enhances hepatic steatosis induced by a high-fat diet and improves insulin sensitivity. Lab Invest 2013;93:311–321

14. Kim B, Do MS, Hyun CK. B-cell-activating factor deficiency attenuates high-fat diet-induced glucose intolerance by potentiating adipose tissue function. Biochem Biophys Res Commun 2015;464:1171–1177

15. Hamada M, Abe M, Miyake T, et al. B cell-activating factor controls the production of adipokines and induces insulin resistance. Obesity (Silver Spring) 2011;19:1915–1922

16. Allman WR, Dey R, Liu L, et al. TACI deficiency leads to alternatively activated macrophage phenotype and susceptibility to Leishmania infection. Proc Natl Acad Sci U S A 2015;112:E4094–E4103

17. Uslu K, Coleman AS, Allman WR, et al. Impaired B cell receptor signaling is responsible for reduced TACI expression and function in X-linked immunodeficient mice. J Immunol 2014;192:3582–3595

18. Anderson EK, Gutierrez DA, Kennedy A, Hasty AH. Weight cycling increases T-cell accumulation in adipose tissue and impairs systemic glucose tolerance. Diabetes 2013;62:3180–3188

19. Sajic T, Hopfgartner G, Szanto I, Varesio E. Comparison of three detergent-free protein extraction protocols for white adipose tissue. Anal Biochem 2011;415:215–217

20. Boge A, Roth RA. A nonradioactive assay for the insulin receptor tyrosine kinase: use in monitoring receptor kinase activity after activation of overexpressed protein kinase C alpha and high glucose treatment. Anal Biochem 1995;231:323–332

21. Heller NM, Gwinn WM, Donnelly RP, Constant SL, Keegan AD. IL-4 engagement of the type I IL-4 receptor complex enhances mouse eosinophil migration to eotaxin-1 in vitro. PLoS One 2012;7:e39673

22. Hardy OT, Czech MP, Corvera S. What causes the insulin resistance underlying obesity? Curr Opin Endocrinol Diabetes Obes 2012;19:81–87

23. Montgomery MK, Hallahan NL, Brown SH, et al. Mouse strain-dependent variation in obesity and glucose homeostasis in response to high-fat feeding. Diabetologia 2013;56:1129–1139

24. Kim YH, Choi BH, Cheon HG, Do MS. B cell activation factor (BAFF) is a novel adipokine that links obesity and inflammation. Exp Mol Med 2009;41:208–216

25. Ferrante AW Jr. The immune cells in adipose tissue. Diabetes Obes Metab 2013;15(Suppl. 3):34–38

26. Lumeng CN, Bodzin JL, Saltiel AR. Obesity induces a phenotypic switch in adipose tissue macrophage polarization. J Clin Invest 2007;117:175–184

27. Wu D, Molofsky AB, Liang HE, et al. Eosinophils sustain adipose alternatively activated macrophages associated with glucose homeostasis. Science 2011;332:243–247

28. Biswas SK, Mantovani A. Macrophage plasticity and interaction with lymphocyte subsets: cancer as a paradigm. Nat Immunol 2010;11:889–896

29. McCormick SM, Heller NM. Regulation of macrophage, dendritic cell, and microglial phenotype and function by the SOCS proteins. Front Immunol 2015;6:549

30. Odegaard JI, Chawla A. Type 2 responses at the interface between immunity and fat metabolism. Curr Opin Immunol 2015;36:67–72

31. Protti A, Mongue-Din H, Mylonas KJ, et al. Bone marrow transplantation modulates tissue macrophage phenotype and enhances cardiac recovery after subsequent acute myocardial infarction. J Mol Cell Cardiol 2016;90:120–128

32. Lumeng CN, DelProposto JB, Westcott DJ, Saltiel AR. Phenotypic switching of adipose tissue macrophages with obesity is generated by spatiotemporal differences in macrophage subtypes. Diabetes 2008;57:3239–3246

33. Amano SU, Cohen JL, Vangala P, et al. Local proliferation of macrophages contributes to obesity-associated adipose tissue inflammation. Cell Metab 2014;19:162–171

34. Rothenberg ME, Hogan SP. The eosinophil. Annu Rev Immunol 2006;24:147–174

35. Kahn SE, Hull RL, Utzschneider KM. Mechanisms linking obesity to insulin resistance and type 2 diabetes. Nature 2006;444:840–846

36. Hotamisligil GS, Peraldi P, Budavari A, Ellis R, White MF, Spiegelman BM. IRS-1-mediated inhibition of insulin receptor tyrosine kinase activity in TNF-alpha- and obesity-induced insulin resistance. Science 1996;271:665–668

37. Senol-Cosar O, Flach RJ, DiStefano M, et al. Tenomodulin promotes human adipocyte differentiation and beneficial visceral adipose tissue expansion. Nat Commun 2016;7:10686

38. Shan B, Wang X, Wu Y, et al. The metabolic ER stress sensor IRE1α suppresses alternative activation of macrophages and impairs energy expenditure in obesity. Nat Immunol 2017;18:519–529

39. Gibala MJ, Little JP, van Essen M, et al. Short-term sprint interval versus traditional endurance training: similar initial adaptations in human skeletal muscle and exercise performance. J Physiol 2006;575:901–911

40. O'Neal TJ, Friend DM, Guo J, Hall KD, Kravitz AV. Increases in physical activity result in diminishing increments in daily energy expenditure in mice. Curr Biol 2017;27:423–430

41. Lee JJ, Rauter I, Garibyan L, et al. The murine equivalent of the A181E TACI mutation associated with common variable immunodeficiency severely impairs B-cell function. Blood 2009;114:2254–2262

42. Saulep-Easton D, Vincent FB, Quah PS, et al. The BAFF receptor TACI controls IL-10 production by regulatory B cells and CLL B cells. Leukemia 2016;30:163–172

43. Chawla A, Nguyen KD, Goh YP. Macrophage-mediated inflammation in metabolic disease. Nat Rev Immunol 2011;11:738–749

44. Dalmas E, Toubal A, Alzaid F, et al. Irf5 deficiency in macrophages promotes beneficial adipose tissue expansion and insulin sensitivity during obesity. Nat Med 2015;21:610–618

45. Han MS, Jung DY, Morel C, et al. JNK expression by macrophages promotes obesity-induced insulin resistance and inflammation. Science 2013;339:218–222

46. Kang K, Reilly SM, Karabacak V, et al. Adipocyte-derived Th2 cytokines and myeloid PPARdelta regulate macrophage polarization and insulin sensitivity. Cell Metab 2008;7:485–495

47. Liao X, Sharma N, Kapadia F, et al. Krüppel-like factor 4 regulates macrophage polarization. J Clin Invest 2011;121:2736–2749

48. Nishimura S, Manabe I, Nagasaki M, et al. CD8+ effector T cells contribute to macrophage recruitment and adipose tissue inflammation in obesity. Nat Med 2009;15:914–920

49. Zheng C, Yang Q, Xu C, et al. CD11b regulates obesity-induced insulin resistance via limiting alternative activation and proliferation of adipose tissue macrophages. Proc Natl Acad Sci U S A 2015;112:E7239–E7248

50. Cogollo E, Silva MA, Isenberg D. Profile of atacicept and its potential in the treatment of systemic lupus erythematosus [published correction appears in Drug Des Devel Ther 2015;9:1865]. Drug Des Devel Ther 2015;9:1331–1339